AGU PUBLICATIONS

Geophysical Research Letters

RESEARCH LETTER
10.1002/2015GL063065

Key Points:
- Glider observations show small diel cycles in dissolved oxygen
- Diel oxygen was used to quantify gross primary productivity
- Chlorophyll, mixing, and temperature also exhibited diel dynamics

Correspondence to:
D. P. Nicholson,
dnicholson@whoi.edu

Citation:
Nicholson, D. P., S. T. Wilson, S. C. Doney, and D. M. Karl (2015), Quantifying subtropical North Pacific gyre mixed layer primary productivity from Seaglider observations of diel oxygen cycles, *Geophys. Res. Lett.*, *42*, 4032–4039, doi:10.1002/2015GL063065.

Received 7 JAN 2015
Accepted 28 APR 2015
Accepted article online 29 APR 2015
Published online 22 MAY 2015

Quantifying subtropical North Pacific gyre mixed layer primary productivity from Seaglider observations of diel oxygen cycles

David P. Nicholson[1,2], Samuel T. Wilson[2,3], Scott C. Doney[1,2], and David M. Karl[2,3]

[1]Marine Chemistry and Geochemistry Department, Woods Hole Oceanographic Institution, Woods Hole, Massachusetts, USA, [2]Daniel K. Inouye Center for Microbial Oceanography: Research and Education, University of Hawaii, Honolulu, Hawaii, USA, [3]Department of Oceanography, University of Hawaii at Manoa, Honolulu, Hawaii, USA

Abstract Using autonomous underwater gliders, we quantified diurnal periodicity in dissolved oxygen, chlorophyll, and temperature in the subtropical North Pacific near the Hawaii Ocean Time-series (HOT) Station ALOHA during summer 2012. Oxygen optodes provided sufficient stability and precision to quantify diel cycles of average amplitude of 0.6 μmol kg^{-1}. A theoretical diel curve was fit to daily observations to infer an average mixed layer gross primary productivity (GPP) of 1.8 mmol O_2 m^{-3} d^{-1}. Cumulative net community production (NCP) over 110 days was 500 mmol O_2 m^{-2} for the mixed layer, which averaged 57 m in depth. Both GPP and NCP estimates indicated a significant period of below-average productivity at Station ALOHA in 2012, an observation confirmed by ^{14}C productivity incubations and O_2/Ar ratios. Given our success in an oligotrophic gyre where biological signals are small, our diel GPP approach holds promise for remote characterization of productivity across the spectrum of marine environments.

1. Introduction

In the surface waters of oligotrophic gyres, net ecosystem metabolism is the result of a tightly coupled balance between photosynthesis and respiration [*Westberry et al.*, 2012; *Ducklow and Doney*, 2013]. In terms of carbon and oxygen, this balance is the sum of gross primary production (GPP), and community respiration (CR) with CR accounting for the sum of respiration by autotrophs (R_A) and heterotrophs (R_H). The residual between GPP and CR, termed net community production (NCP), is of much smaller magnitude (by 10–20 times) than either GPP or CR. NCP is a critical term in the global carbon cycle as it represents the material that can eventually be exported via the biological pump and hence is a net biological sink for CO_2. NCP and the biological pump provide the fuel that supports low-energy mesopelagic ecosystems below the euphotic zone. Scenarios of climate change over the 21st century predict increased stratification, warming, and reduced nutrients in oligotrophic gyres [*Bopp et al.*, 2013; *Boyd et al.*, 2015]. The amalgam of changes to each metabolic process (GPP, R_A, and R_H) will dictate how NCP will change in the future. Metabolic rates increase with temperature, but respiration does more so than photosynthesis, which could shift metabolic balance toward heterotrophy [*Brown et al.*, 2004; *López-Urrutia et al.*, 2006]. Given the already low rates of biological activity in oligotrophic gyres, quantifying NCP is a considerable challenge. If NCP is estimated by differencing GPP and CR, a small, systematic error in methodology for quantifying either GPP or CR can result in a significant bias in inferred NCP [*Williams et al.*, 2004; *Quay et al.*, 2010]. Bottle effects inherent to incubation-based approaches are one potential source of such bias. Uncertainties and discrepancies in quantifying these rates in the ocean have led to ongoing disagreement regarding the overall metabolic state of the subtropical ocean [*Duarte et al.*, 2013; *Ducklow and Doney*, 2013; *Williams et al.*, 2013]. Oxygen is a commonly utilized tracer of ocean metabolism, as it is produced during photosynthesis and consumed during respiration. Variations in biological oxygen cycling over the diel period can be interpreted to infer GPP and CR based on assumptions of photosynthetic oxygen production during daytime and respiratory consumption at night. In the ocean, this approach has been applied using O_2/Ar, which partially corrects for physically driven O_2 variability. Large-amplitude diel O_2/Ar signals have been observed in the high-latitude Southern Ocean [*Hamme et al.*, 2012; *Tortell et al.*, 2014]; and more recently, GPP and CR have been quantified in the subtropical North Pacific using O_2/Ar [*Ferrón et al.*, 2015]. While O_2/Ar helps to isolate the biological signal from physical variability in dissolved O_2, it is also possible to quantify diel periodicity in dissolved oxygen directly. Through laborious Winkler titration, a diel oxygen cycle of ~1 μmol kg^{-1} was observed over a day at five stations in the subtropical Atlantic [*Tijssen*, 1979].

Fortunately, improvements in sensor and autonomous platform technology enable a considerable expansion of the temporal and spatial scope of such observations. For example, *Johnson* [2010] quantified primary productivity in Monterey Bay using moored oxygen, nitrate, and pCO_2 sensors. Community respiration was estimated from an oxygen sensor on a wave glider for a section through the Pacific [*Wilson et al*., 2014].

Here we apply observations from an autonomous underwater glider [*Eriksen et al*., 2001] to explore the diurnal dynamics of oxygen in the mixed layer near the time series site, Station ALOHA [*Karl and Lukas*, 1996], during the 2012 Hawaii Ocean Experiment Dynamics of Light and Nutrients (HOE-DYLAN) experiment. We quantify depth-resolved GPP and CR from upper ocean glider profiles spanning 22 May to 8 September 2012. In addition to oxygen, we explore diurnal cyclicity in chlorophyll fluorescence and temperature and investigate the diel rhythm of air-sea O_2 flux and active mixing within the surface ocean boundary layer.

2. Observations

2.1. Glider

During 2012, two C-MORE Seagliders [*Eriksen et al*., 2001] (sg146 and sg148) were deployed to monitor the area near Station ALOHA. Each glider sampled a "bowtie" shaped pattern inscribed within a nominal 50 by 50 km square. Station ALOHA (22.75°N, 158.00°W) is located near the southwest corner of the sample region. Each glider repeatedly profiled in a sawtooth manner to a depth of 600–700 m. The shallower inflection near 600 m, rather than the 1000 m depth that has been more typical for glider deployments in the region [*Nicholson et al*., 2008], was designed to improve temporal and spatial resolution within the euphotic zone. All sensors sampled at 1/6 Hz in the upper 200 m with reduced sampling frequency for the optical puck below 200 m resulting in <1 m vertical resolution through the euphotic zone. With a 600 m inflection depth, the glider obtained approximately seven dives and seven ascents (14 profiles) per day, sufficient to characterize oscillations in the diurnal band. The gliders were equipped with Aanderaa optode dissolved oxygen sensors (AADI 3830), Seabird Electronics Clark polarographic membrane-type oxygen sensors (SBE-43), optical triplet pucks for chlorophyll fluorescence, backscatter, and Colored Dissolved Organic Matter (CDOM) (WET Labs ECO). For the purpose of observing diel cycles, the lower noise of the Aanderaa optodes proved superior to the SBE-43 sensors, which were unable to reliably resolve diel cycles. Oxygen saturation anomaly (ΔO_2) was calculated from dissolved oxygen and temperature and salinity dependent saturation state [*Garcia and Gordon*, 1992]. A single constant oxygen offset was applied for each glider to minimize saturation anomaly differences between factory calibration and mixed layer oxygen Winkler titrations from HOT and HOE-DYLAN cruises using all Winkler observations within 5 km and 2 days of a glider profile. Offsets were $15.9 \pm 1.3\ \mu mol\ kg^{-1}$ ($n = 7$) for sg146 and $7.5 \pm 1.5\ \mu mol\ kg^{-1}$ ($n = 26$) for sg148. Error estimates are based on 1 standard deviation of the difference between calibrated sensor O_2 and matched Winkler O_2. No statistically significant trend in calibration offset was observed over the duration of either deployment. The calibration procedure has no effect on the calculated magnitude of diurnal oxygen cycles but is important for NCP calculations.

2.2. Mooring

We augment Seaglider observations with data from the nearby Woods Hole Oceanographic Institution Hawaii Ocean Time-series Site (WHOTS) mooring located at 22.7678°N, 157.9882°W (www.soest.hawaii.edu/whots/). WHOTS mooring instrumentation used includes upward looking acoustic Doppler current profilers (ADCPs) at 47.5 m and 125 m (Rockland Scientific Workhorse 600 kHz and 300 kHz, respectively) as well as meteorological measurements of wind speed and sea level pressure from WHOT deployment #8 (7 July 2011 to 16 June 2012) and #9 (14 June 2012 to 14 June 2013).

3. Results and Discussion

Throughout the study period, oxygen was slightly supersaturated within the mixed layer (101–102%). Mixed layer depth defined using a $0.125\ kg\ m^{-3}$ density offset threshold relative to a 10 m reference depth ($h^{\Delta\sigma = 0.125}$) varied from around 40–80 m (average was 57 m). As is typical of the subtropical ocean, oxygen saturation increased directly below the mixed layer, within the sunlit upper thermocline, here reaching saturation levels of about 106% due to combined effects of photosynthesis and heating [*Shulenberger and Reid*, 1981; *Spitzer and Jenkins*, 1989; *Emerson et al*., 1995]. At Station ALOHA, submixed layer production

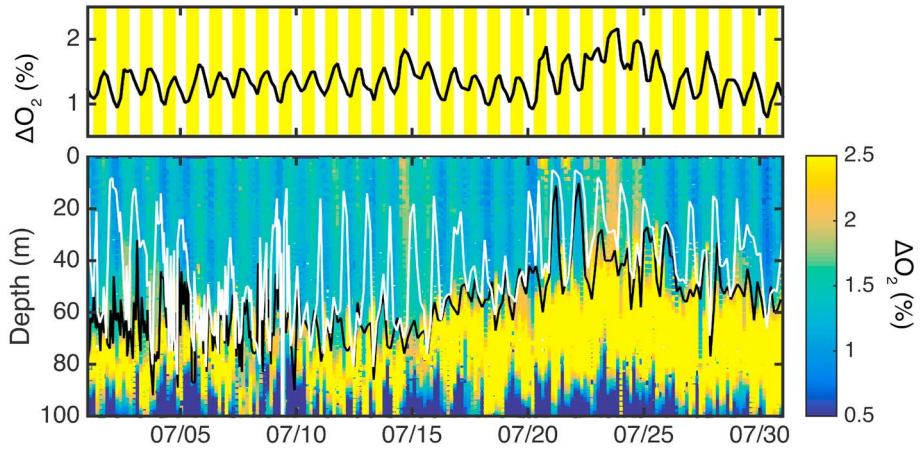

Figure 1. Oxygen saturation anomaly (%) is shown averaged over the upper 40 m (above) and through the upper 100 m (below) for the month of July 2012. Yellow bars (above) show daylight hours. Below, mixed layer depth using a density threshold ($\Delta\sigma_\theta$) of 0.03 kg m^{-3} and 0.125 kg m^{-3} is plotted in white and black, respectively.

has been estimated to account for about 25% of total euphotic zone NCP [*Emerson et al.*, 2008; *Nicholson et al.*, 2008; *Riser and Johnson*, 2008], consistent with incubation-based estimates of the fraction of primary production occurring at depth [*Quay et al.*, 2010]. On the diel time scale, oscillations in mixed layer O_2 saturation on the order of ±0.3% (0.6 μmol kg^{-1}) were evident (Figure 1).

We investigated the vertical structure and timing of diel cycles using superposed epoch analysis to composite Seaglider observations over the 24 h period along depth horizons through the mixed layer. To calculate composites, we performed the following steps: (1) each glider profile was linearly interpolated in depth to 1 m horizons; (2) for each horizon, daily mean values were subtracted from each data point, and (3) resultant daily anomalies were binned and averaged for each hourly interval through the day (Figure 2). As expected, oxygen reached a minimum near sunrise, and maximum near sunset. Temperature exhibited a similar cycle, due to diurnal heating and stratification. Chlorophyll fluorescence was minimum near noon, and highest at night, presumably due to fluorescence quenching as has previously been observed from a Seaglider [*Perry*

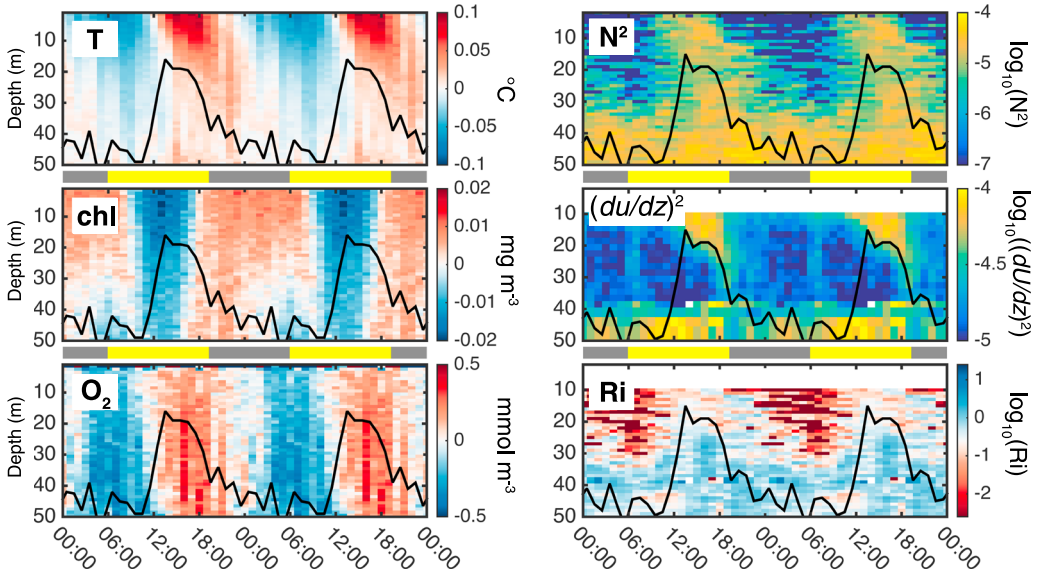

Figure 2. Composite daily anomalies over the upper 50 m and 110 day study period are shown for (left column) temperature (T), chlorophyll (chl), and oxygen (O_2). (right column) Squared Brunt Väisälä frequency (N^2), shear squared $(du/dz)^2$ from WHOTS ADCPs, and Richardson number (Ri), derived from N^2 and $(du/dz)^2$. The black line indicates average hourly mixed layer depth using a 0.03 kg m^{-3} $\Delta\sigma_\theta$ threshold, and grey and gold bars represent nighttime and daylight hours for July 1.

et al., 2008]. The magnitudes of both temperature and chlorophyll cycles were surface intensified, while oxygen was relatively uniform through the upper 40 m. For temperature, trough to peak amplitude of diel oscillations decreased from 0.17°C at 5 m to 0.02°C at 40 m. For chlorophyll fluorescence, amplitude decreased from 0.03 mg m^{-3} at 5 m to 0.01 mg m^{-3} at 40 m for chlorophyll. For oxygen, amplitude increased slightly with depth from 0.5 μmol kg^{-1} at 5 m to 0.8 μmol kg^{-1} at 40 m.

3.1. Diel Mixing and Stratification

Mixed layer depth (MLD), most commonly defined by a density criterion [*de Boyer Montégut et al*., 2004], does not necessarily represent the depth of active mixing layer (XLD) within the minimally stratified surface ocean boundary layer [*Sutherland et al*., 2014]. MLD at Station ALOHA traditionally has been defined by a density offset threshold of 0.125 kg m^{-3} [*Karl and Lukas*, 1996]. From Seaglider profiles, we also apply a more stringent threshold of $\Delta\sigma_\theta = 0.03$ kg m^{-3} ($h^{\Delta\sigma = 0.03}$) [*de Boyer Montégut et al*., 2004]. Diurnal heating, cooling, and wind forcing result in daytime stratification, such that XLD is shallower than the bulk mixed layer, MLD [*Price et al*., 1986]. The Richardson (*Ri*) number is a useful metric to evaluate if stratification and shear conditions are conducive to shear instability driven mixing and is defined as

$$Ri = \frac{N^2}{(\mathrm{d}u/\mathrm{d}z)^2} \tag{1}$$

where N is the Brunt-Väisälä frequency and (du/dz) is the vertical current shear [*Large et al*., 1994]. A Richardson number below a critical value ($Ri_{crit} = 0.25$) describe conditions under which shear is sufficient to overcome stratification. We calculated N from the density structure from Seaglider observations and shear from WHOTS ADCPs. Seaglider and WHOTS data were linearly interpolated and combined to calculate Richardson number (Figure 2). Stratification tended to have a minimum near dawn and increased through daytime hours, while there was a maximum in near-surface shear in the afternoon/evening confined to the region shallower than $h^{\Delta\sigma = 0.03}$. Richardson number below Ri_{crit} was observed to extend on average to a depth of 20 m near sunset and to a depth of 33 m near dawn. We find that at Station ALOHA $h^{\Delta\sigma = 0.03}$ is a suitable choice to approximate XLD.

3.2. Air-Sea Exchange and Net Community Production

Mixed layer NCP can be estimated by quantifying the net air-sea flux of oxygen from the mixed layer [*Emerson et al*., 2008]. We calculated air-sea flux using hourly meteorological forcing (wind speed and atmospheric pressure) from the WHOTS buoy in combination with oxygen, temperature, and salinity measurements from Seagliders. We calculated mixed layer biological O_2 flux following *Emerson et al*. [2008] using a recent parameterization that includes explicit bubble flux terms [*Liang et al*., 2013]. Bubble mediated air-sea flux maintains a physically driven supersaturation of oxygen at steady state [*Keeling*, 1993; *Schudlich and Emerson*, 1996]. Without explicit consideration of bubble-mediated supersaturation, NCP can be significantly overestimated. Over the 110 day total deployment period for sg146 and sg148 (22 May to 8 September), cumulative NCP was 500 ± 400 mmol O_2 m^{-2}. The uncertainty estimate was based on assuming a 20% uncertainty in gas transfer coefficient [*Wanninkhof*, 2014], a 100% uncertainty in the air-sea bubble flux and a 0.5 μmol kg^{-1} uncertainty in sensor offset (based on standard error of the mean for sg146, which was higher than for sg148). For the near-equilibrium conditions we observed, sensor offset was the largest source of uncertainty (±340 mmol O_2 m^{-2}) followed by bubble flux (±220 mmol O_2 m^{-2}) and gas transfer coefficient (±140 mmol O_2 m^{-2}). Extrapolating to an annual rate yields 1700 mmol m^{-2} yr^{-1} which likely is an overestimate given typically lower wintertime productivity. Even so, this NCP value is on the low end of previously reported mixed layer NCP for Station ALOHA, such as an annual rate of 5100 mmol O_2 m^{-2} yr^{-1}in 2006–2008 [*Quay et al*., 2010], 4800 mmol O_2 m^{-2} yr^{-1} in 2005 [*Emerson et al*., 2008], 1600 mmol O_2 m^{-2} yr^{-1} in 2000 and 2001 [*Hamme and Emerson*, 2006], and 2100 mmol O_2 m^{-2} yr^{-1}, 3900 mmol O_2 m^{-2} yr^{-1}, and 3900 mmol O_2 m^{-2} yr^{-1} in 1990, 1992, and 1995, respectively [*Emerson et al*., 1997]. Given that we quantified productivity at Station ALOHA during summer when productivity is historically highest, we conclude that the summer of 2012 had an anomalously low rate of NCP.

Because air-sea flux is a function of surface oxygen saturation, diel variations in oxygen result in a diel cycle in air-sea gas flux. Sea to air flux is maximal when ΔO_2 is maximal, shortly before sunset. The effect of this flux on the time rate of change of mixed layer oxygen ($(dO_2/dt)^{ge}$) is further amplified because the timing of shallowest

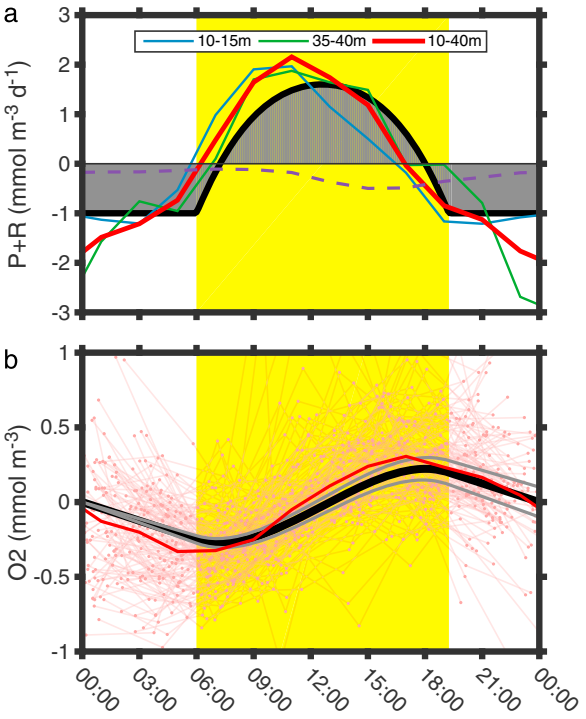

Figure 3. (a) The sum of photosynthesis and respiration (GPP + CR) through the diel period as derived from equations (2) and (3) is shown for 15 July (above) with shaded region highlighting when the system is net autotrophic and heterotrophic. Colored lines show composite of Seaglider observations for 10–40 m (red), 10–15 m (blue), and 35–40 m (green), illustrating the slightly earlier timing of the diel cycle in near-surface waters. Purple line shows the volumetric oxygen flux due to gas exchange ($(dO_2/dt)^{ge}$). (b) The integral of the above curve is the calculated diel O_2 cycle for GPP = 1.0 mmol O_2 m^{-3} d^{-1} (below) and has an amplitude of ±0.25 mmol O_2 m^{-3}. The integral of the observed 10–40 m curve is shown below in thick red, while thin red lines show the O_2 cycles from each day with mean removed. Gray lines are the result when CR is increased (heterotrophic conditions) or decreased (autotrophic conditions) by 10%.

$h^{\Delta\sigma=0.03}$ is coincident with the maximum in ΔO_2 (Figure 3; see also Appendix C in *Keeling et al*. [1998]). Air-sea flux results in a dO_2/dt less than 0.2 mmol O_2 m^{-3} d^{-1} which is considerably smaller than rates of GPP. We correct for this term in our GPP calculation.

3.3. GPP From Diel Oxygen

The expected shape of an idealized diel cycle in dissolved oxygen depends upon time-varying photosynthesis (*P*) and irradiance (*E*) such that

$$P = P_m\left(1 - e^{-E/E_k}\right) \quad \text{where } E_k = P_m/\alpha \quad (2)$$

where P_m is the maximum rate of photosynthesis, E_k is the saturating irradiance, and α is the initial slope [*Jassby and Platt*, 1976]. Irradiance through the day was approximated based on solar altitude

$$E(t) = E_0 \cos(\theta(t)) \quad (3)$$

where E_0 is mean mixed layer integrated irradiance if the Sun was directly overhead, θ_s is the solar elevation angle, and *t* is time. Using equations (2) and (3) and representative values for E_k (150 μmol quanta m^{-2} s^{-1}) and E_0 (150 μmol quanta m^{-2} s^{-1}) for the subtropical North Pacific [*Ondrusek et al*., 2001; *Li et al*., 2011], we calculated a diel photosynthesis curve with a daily-integrated GPP of 1 mmol O_2 m^{-3} d^{-1} (Figure 3). The magnitudes of diel curves are very insensitive to the choice of E_k (150 μmol quanta m^{-2} s^{-1}) and E_0. Assuming CR of constant magnitude and daily-integrated value equaling GPP [*Kosten et al*., 2014], we determined that the resulting theoretical diel oxygen curve had a trough to peak magnitude of 0.50 mmol O_2 m^{-3} (Figure 3). For an autotrophic system (GPP > CR), the theoretical diel curve would result in a net increase of O_2, and vice versa for a heterotrophic system (Figure 3b), although excess oxygen can leave the system via air-sea gas exchange. A composite curve was created from Seaglider observations by calculating the gradient between consecutive observations along a depth horizon and binning into hourly median estimates of dO_2/dt (Figure 3). Compared to the theoretical curve, observed O_2 production at 10 m peaks earlier in the day, while at 40 m, photosynthesis through the day appears to better fit the theoretical curve. An asymmetric morning peak in diel rates of photosynthesis has long been recognized [e.g., *Marra*, 1978] which may explain the early timing of the peak observed in Figure 3. During night, O_2 consumption is reduced in predawn hours. It is unclear if the observed deviations from the theoretical curve are primarily biological, or if diel physical processes contribute. For example, *h* is deepest during predawn hours and may entrain supersaturated waters from below, which would have a similar effect as reduced respiration rates in predawn hours.

Physically driven variability in O_2, such as submesoscale fronts or entrainment events, potentially could be misattributed to diel productivity. To minimize such misattribution, we required observations to fit the theoretical shape and timing of diel photosynthesis and respiration. Before fitting to the theoretical curve,

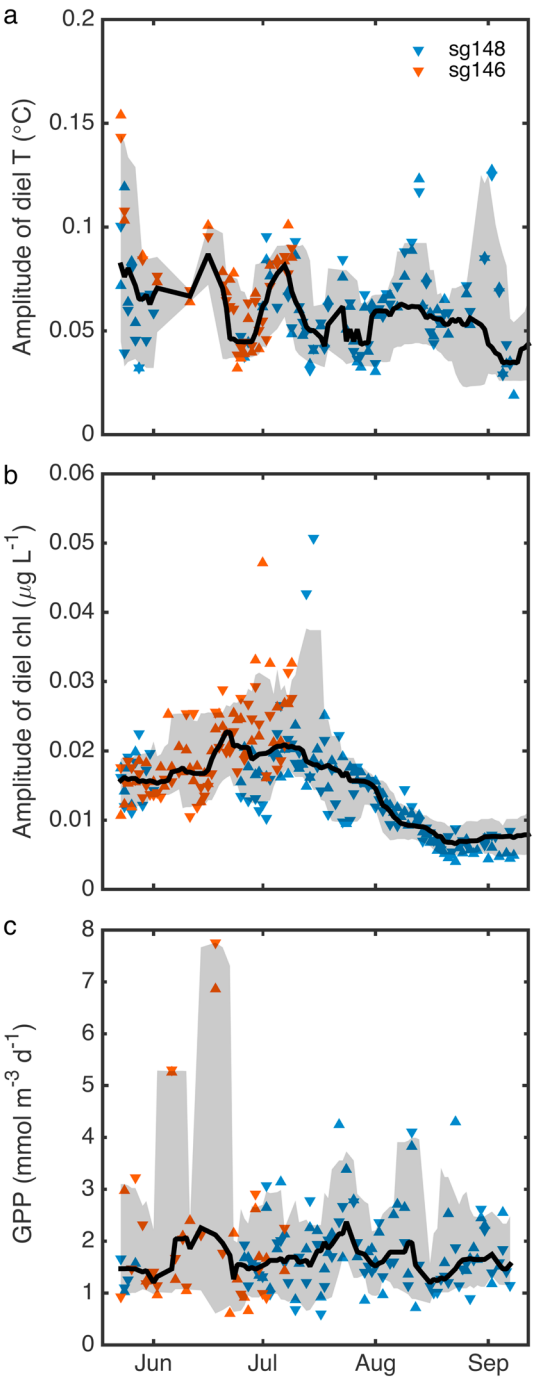

Figure 4. The amplitude of diel cycles fit from each glider is shown for (a) temperature at 10 m, (b) chlorophyll fluorescence at 10 m, and (c) GPP averaged from 0 to 40 m. Black lines show a 9 day running median window. Shaded regions encompass 25th–75th percentiles of the 9 day running median. Upward pointing arrows are calculated from Seaglider ascents, and downward arrows from dives.

we accounted for air-sea exchange by adding O_2 efflux ($(dO_2/dt)^{ge}$) back to the observed mixed layer diel cycle after which data from each day were detrended. These steps had only minor impact on calculated GPP (e.g., detrending only changed average GPP by $< 3\%$) but may be more important in regions where GPP and CR are not so tightly coupled. Observed changes in mixed layer dissolved oxygen for each day were fitted to our calculated diel curve allowing for two parameters to be optimized for each day, one for amplitude (A) and one for phase (φ), by minimizing the cost function:

$$\min_{A,\varphi}\left(\frac{1}{N}\sum_{i=1}^{N}(o_i - Af(t_i+\varphi))^2\right) \quad (4)$$
$$\text{subject to } A \geq 0 \text{ and } |\varphi| \leq 4 \text{ hr}$$

where N is the number of observations in a day, o_i is observed O_2, t_i is the time of observations, and $f(t)$ is the diel O_2 curve calculated from equations (2) and (3). A phase requirement of ± 4 h ensured that within a day, minimum O_2 preceded maximum O_2 at close to predicted timing. Since $f(t)$ was calculated using daily GPP of 1 mmol $O_2\,m^{-3}\,d^{-1}$, the A derived for each day is equal to the GPP for that day. The resulting daily fits were evaluated for statistical significance using a t test with N - 2 degrees of freedom ($p < 0.05$). Because minor hysteresis effects can cause offset between data from dives and ascents [*Nicholson et al.*, 2008], dive and ascent data were fit separately to obtain two independent estimates of diel amplitude per glider, per day. A similar fitting procedure was applied for other glider variables, with a sine curve used for fitting, rather than the diel curve.

Of the 110 daily measurements conducted by sg146 and sg148, 73 days showed a statistically significant fit to the theoretical diel O_2 photosynthesis curve ($p < 0.05$). As evident in Figure 3, phase for these days averaged about an hour earlier than expected ($\phi = 1.0 \pm 1.6$ h). In addition to oxygen, temperature and chlorophyll fluorescence also exhibited diel variability. No diel signal was evident in other sensor data, including backscatter, CDOM, and salinity. Mean mixed layer GPP over the observation period was 1.8 ± 0.7 mmol $O_2\,m^{-3}\,d^{-1}$. GPP showed no significant trend over the study period but did show occasional "high productivity" days with inferred GPP sometimes exceeding 4 mmol $O_2\,m^{-3}\,d^{-1}$ (Figure 4). HOE-DYLAN included incubation-based ^{14}C primary productivity for 43 days spanning late June through mid-September, which averaged 0.58 ± 0.08 mmol $C\,m^{-3}\,d^{-1}$. For these days, the resulting average GPP_{O2}:PP_C was 3.2,

which is consistent with estimates based on oxygen isotope tracers at Station ALOHA [*Quay et al.*, 2010; *Nicholson et al.*, 2012].

4. Conclusions

Diel variations in surface ocean dissolved oxygen bear the imprint of photosynthesis and respiration. The combination of a profiling glider and optode oxygen sensor was sufficient to robustly identify diel cycles as small as $\pm 0.2\,\mu mol\,kg^{-1}$. Surface-intensified diel cycles in temperature and chlorophyll fluorescence also were observed. Based on the diel O_2 signal, we quantified GPP and CR in the oligotrophic subtropical gyre, which averaged $1.8\,mmol\,O_2\,m^{-2}\,d^{-1}$. GPP averaged 3.2 times incubation-based PP(^{14}C) during the same period. NCP during the same period was unusually low, amounting to less than 5% of GPP.

Such methods must be applied with care in order to limit uncertainty as they are quite sensitive to sensor performance. For estimating GPP, a precise and low-noise O_2 sensor is critical, as is consideration of physically driven variability. For NCP, absolute accuracy via calibration and long-term stability of the O_2 sensor are paramount. Rates of primary productivity are severely undersampled in the ocean, and careful application of autonomous in situ approaches such as presented here opens new avenues to quantifying GPP, CR, and NCP in a wide range of ocean environments.

Acknowledgments

The authors acknowledge support from the National Science Foundation (NSF) through an NSF Science and Technology Center, the Center for Microbial Oceanography Research and Education (C-MORE; NSF EF-0424599). D.N. also was supported by NSF (OCE-1129644) and an Independent Study Award from the Woods Hole Oceanographic Institution (WHOI). D.M. K. was also supported by the Gordon and Betty Moore Foundation. WHOI Summer Student Fellow Cole Stites-Clayton, Stanford University, contributed to early stages of Seaglider data analysis and was supported by an NSF REU grant to WHOI (OCE-1156952). Data from the WHOTS surface mooring are gratefully acknowledged; the NOAA Climate Observation Division provides funding to Robert A. Weller and Albert J. Plueddemann at WHOI to support the long-term deployment of the surface mooring. At the University of Hawaii, Steve Poulos led field operations and piloting for the Seagliders and Matt Church provided ^{14}C primary productivity data. Seaglider and WHOTS data are available at http://hahana.soest.hawaii.edu/seagliders/ and http://www.soest.hawaii.edu/whots/, respectively. We also thank the thoughtful contributions of two anonymous reviewers.

The Editor thanks two anonymous reviewers for their assistance in evaluating this paper.

References

Bopp, L., et al. (2013), Multiple stressors of ocean ecosystems in the 21st century: Projections with CMIP5 models, *Biogeosciences*, *10*(10), 6225–6245, doi:10.5194/bg-10-6225-2013.

Boyd, P. W., S. T. Lennartz, D. M. Glover, and S. C. Doney (2015), Biological ramifications of climate-change-mediated oceanic multi-stressors, *Nat. Clim. Change*, *5*(1), 71–79, doi:10.1038/nclimate2441.

Brown, J. H., J. F. Gillooly, A. P. Allen, V. M. Savage, and G. B. West (2004), Toward a metabolic theory of ecology, *Ecology*, *85*(7), 1771–1789, doi:10.1890/03-9000.

De Boyer Montégut, C., G. Madec, A. S. Fischer, A. Lazar, and D. Iudicone (2004), Mixed layer depth over the global ocean: An examination of profile data and a profile-based climatology, *J. Geophys. Res.*, *109*, C12003, doi:10.1029/2004JC002378.

Duarte, C. M., A. Regaudie-de-Gioux, J. M. Arrieta, A. Delgado-Huertas, and S. Agustí (2013), The oligotrophic ocean is heterotrophic*, *Annu. Rev. Mar. Sci.*, *5*(1), 551–569, doi:10.1146/annurev-marine-121211-172337.

Ducklow, H. W., and S. C. Doney (2013), What is the metabolic state of the oligotrophic ocean? A debate, *Annu. Rev. Mar. Sci.*, *5*(1), 525–533, doi:10.1146/annurev-marine-121211-172331.

Emerson, S., P. D. Quay, C. Stump, D. Wilbur, and R. Schudlich (1995), Chemical tracers of productivity and respiration in the subtropical Pacific Ocean, *J. Geophys. Res.*, *100*, 15,873–15,887, doi:10.1029/95JC01333.

Emerson, S., P. Quay, D. Karl, C. Winn, L. Tupas, and M. Landry (1997), Experimental determination of the organic carbon flux from open-ocean surface waters, *Nature*, *389*(6654), 951–954, doi:10.1038/40111.

Emerson, S., C. Stump, and D. Nicholson (2008), Net biological oxygen production in the ocean: Remote in situ measurements of O_2 and N^2 in surface waters, *Global Biogeochem. Cycles*, *22*, GB3023, doi:10.1029/2007GB003095.

Eriksen, C. C., T. J. Osse, R. D. Light, T. Wen, T. W. Lehman, P. L. Sabin, J. W. Ballard, and A. M. Chiodi (2001), Seaglider: A long-range autonomous underwater vehicle for oceanographic research, *IEEE J. Oceanic Eng.*, *26*(4), 424–436.

Ferrón, S., S. T. Wilson, S. Martínez-García, P. D. Quay, and D. M. Karl (2015), Metabolic balance in the mixed layer of the oligotrophic North Pacific Ocean from diel changes in O_2/Ar saturation ratios, *Geophys. Res. Lett.*, *42*, doi:10.1002/2015GL063555, in press.

Garcia, H. E., and L. I. Gordon (1992), Oxygen solubility in seawater: Better fitting equations, *Limnol. Oceanogr.*, *37*(6), 1307–1312, doi:10.4319/lo.1992.37.6.1307.

Hamme, R. C., and S. R. Emerson (2006), Constraining bubble dynamics and mixing with dissolved gases: Implications for productivity measurements by oxygen mass balance, *J. Mar. Res.*, *64*(1), 73–95, doi:10.1357/002224006776412322.

Hamme, R. C., et al. (2012), Dissolved O_2/Ar and other methods reveal rapid changes in productivity during a Lagrangian experiment in the Southern Ocean, *J. Geophys. Res.*, *117*, C00F12, doi:10.1029/2011JC007046.

Jassby, A. D., and T. Platt (1976), Mathematical formulation of the relationship between photosynthesis and light for phytoplankton, *Limnol. Oceanogr.*, *21*(4), 540–547, doi:10.4319/lo.1976.21.4.0540.

Johnson, K. S. (2010), Simultaneous measurements of nitrate, oxygen, and carbon dioxide on oceanographic moorings: Observing the Redfield ratio in real time, *Limnol. Oceanogr.*, *55*(2), 615–627, doi:10.4319/lo.2010.55.2.0615.

Karl, D. M., and R. Lukas (1996), The Hawaii Ocean Time-series (HOT) program: Background, rationale and field implementation, *Deep Sea Res., Part II*, *43*(2–3), 129–156, doi:10.1016/0967-0645(96)00005-7.

Keeling, R. F. (1993), On the role of large bubbles in air-sea gas exchange and supersaturation in the ocean, *J. Mar. Res.*, *51*(2), 237–271, doi:10.1357/0022240933223800.

Keeling, R. F., B. B. Stephens, R. G. Najjar, S. C. Doney, D. Archer, and M. Heimann (1998), Seasonal variations in the atmospheric O_2/N^2 ratio in relation to the kinetics of air-sea gas exchange, *Global Biogeochem. Cycles*, *12*(1), 141–163, doi:10.1029/97GB02339.

Kosten, S., B. O. L. Demars, and B. Moss (2014), Distinguishing autotrophic and heterotrophic respiration based on diel oxygen change curves: Revisiting Dr. Faustus, Freshw, *Biology*, *59*(3), 649–651, doi:10.1111/fwb.12288.

Large, W. G., J. C. McWilliams, and S. C. Doney (1994), Oceanic vertical mixing: A review and a model with a nonlocal boundary layer parameterization, *Rev. Geophys.*, *32*(4), 363–403, doi:10.1029/94RG01872.

Li, B., D. M. Karl, R. M. Letelier, and M. J. Church (2011), Size-dependent photosynthetic variability in the North Pacific subtropical gyre, *Mar. Ecol. Prog. Ser.*, *440*, 27–40, doi:10.3354/meps09345.

Liang, J.-H., C. Deutsch, J. C. McWilliams, B. Baschek, P. P. Sullivan, and D. Chiba (2013), Parameterizing bubble-mediated air-sea gas exchange and its effect on ocean ventilation, *Global Biogeochem. Cycles*, *27*, 894–905, doi:10.1002/gbc.20080.

López-Urrutia, Á., E. S. Martin, R. P. Harris, and X. Irigoien (2006), Scaling the metabolic balance of the oceans, *Proc. Natl. Acad. Sci. U.S.A.*, *103*(23), 8739–8744, doi:10.1073/pnas.0601137103.

Marra, J. (1978), Effect of short-term variations in light intensity on photosynthesis of a marine phytoplankter: A laboratory simulation study, *Mar. Biol.*, *46*(3), 191–202, doi:10.1007/BF00390680.

Nicholson, D., S. Emerson, and C. C. Eriksen (2008), Net community production in the deep euphotic zone of the subtropical North Pacific gyre from glider surveys, *Limnol. Oceanogr.*, *53*(5_part_2), 2226–2236, doi:10.4319/lo.2008.53.5_part_2.2226.

Nicholson, D., R. H. R. Stanley, E. Barkan, D. M. Karl, B. Luz, P. D. Quay, and S. C. Doney (2012), Evaluating triple oxygen isotope estimates of gross primary production at the Hawaii Ocean Time-series and Bermuda Atlantic Time-series study sites, *J. Geophys. Res.*, *117*, C05012, doi:10.1029/2010JC006856.

Ondrusek, M. E., R. R. Bidigare, K. Waters, and D. M. Karl (2001), A predictive model for estimating rates of primary production in the subtropical North Pacific Ocean, *Deep Sea Res., Part II*, *48*(8–9), 1837–1863, doi:10.1016/S0967-0645(00)00163-6.

Perry, M. J., B. S. Sackmann, C. C. Eriksen, and C. M. Lee (2008), Seaglider observations of blooms and subsurface chlorophyll maxima off the Washington coast, *Limnol. Oceanogr.*, *53*(5part2), 2169–2179, doi:10.4319/lo.2008.53.5_part_2.2169.

Price, J. F., R. A. Weller, and R. Pinkel (1986), Diurnal cycling: Observations and models of the upper ocean response to diurnal heating, cooling, and wind mixing, *J. Geophys. Res.*, *91*(C7), 8411–8427, doi:10.1029/JC091iC07p08411.

Quay, P. D., C. Peacock, K. Björkman, and D. M. Karl (2010), Measuring primary production rates in the ocean: Enigmatic results between incubation and non-incubation methods at Station ALOHA, *Global Biogeochem. Cycles*, *24*, GB3014, doi:10.1029/2009GB003665.

Riser, S. C., and K. S. Johnson (2008), Net production of oxygen in the subtropical ocean, *Nature*, *451*(7176), 323–325.

Schudlich, R., and S. Emerson (1996), Gas supersaturation in the surface ocean: The roles of heat flux, gas exchange, and bubbles, *Deep Sea Res., Part II*, *43*(2–3), 569–589.

Shulenberger, E., and J. L. Reid (1981), The Pacific shallow oxygen maximum, deep chlorophyll maximum, and primary productivity, reconsidered, *Deep Sea Res., Part A*, *28*(9), 901–919, doi:10.1016/0198-0149(81)90009-1.

Spitzer, W. S., and W. J. Jenkins (1989), Rates of vertical mixing, gas exchange and new production: Estimates from seasonal gas cycles in the upper ocean near Bermuda, *J. Mar. Res.*, *47*(1), 169–196.

Sutherland, G., G. Reverdin, L. Marié, and B. Ward (2014), Mixed and mixing layer depths in the ocean surface boundary layer under conditions of diurnal stratification, *Geophys. Res. Lett.*, *41*, 8469–8476, doi:10.1002/2014GL061939.

Tijssen, S. B. (1979), Diurnal oxygen rhythm and primary production in the mixed layer of the Atlantic Ocean at 20°N, *Neth. J. Sea Res.*, *13*(1), 79–84, doi:10.1016/0077-7579(79)90034-6.

Tortell, P. D., E. C. Asher, H. W. Ducklow, J. A. L. Goldman, J. W. H. Dacey, J. J. Grzymski, J. N. Young, S. A. Kranz, K. S. Bernard, and F. M. M. Morel (2014), Metabolic balance of coastal Antarctic waters revealed by autonomous pCO_2 and ΔO_2/Ar measurements, *Geophys. Res. Lett.*, *41*, 6803–6810, doi:10.1002/2014GL061266.

Wanninkhof, R. (2014), Relationship between wind speed and gas exchange over the ocean revisited, *Limnol. Oceanogr. Methods*, *12*(6), 351–362, doi:10.4319/lom.2014.12.351.

Westberry, T. K., P. J. l. B. Williams, and M. J. Behrenfeld (2012), Global net community production and the putative net heterotrophy of the oligotrophic oceans, *Global Biogeochem. Cycles*, *26*, GB4019, doi:10.1029/2011GB004094.

Williams, P. J. l. B., P. J. Morris, and D. M. Karl (2004), Net community production and metabolic balance at the oligotrophic ocean site, station ALOHA, *Deep Sea Res., Part A*, *51*(11), 1563–1578, doi:10.1016/j.dsr.2004.07.001.

Williams, P. J. l. B., P. D. Quay, T. K. Westberry, and M. J. Behrenfeld (2013), The oligotrophic ocean is autotrophic, *Annu. Rev. Mar. Sci.*, *5*(1), 535–549, doi:10.1146/annurev-marine-121211-172335.

Wilson, J. M., R. Severson, and J. M. Beman (2014), Ocean-scale patterns in community respiration rates along continuous transects across the Pacific Ocean, *PLoS One*, *9*(7), e99821, doi:10.1371/journal.pone.0099821.